HHS Public Access

Author manuscript

Bioconjug Chem. Author manuscript; available in PMC 2017 September 21.

Published in final edited form as:

Bioconjug Chem. 2016 September 21; 27(9): 2157–2165. doi:10.1021/acs.bioconjchem.6b00374.

Design, Synthesis and Evaluation of a Neurokinin 1 Receptor-Targeted Near IR Dye for Fluorescence Guided Surgery of Neuroendocrine Cancers

Ananda Kumar Kanduluru, **Madduri Srinivasarao**, and **Philip S Low***

Department of Chemistry and Institute for Drug Discovery, Purdue University, West Lafayette, Indiana 47907, United States

Abstract

The neurokinin-1 receptor (NK1R) is implicated in the growth and metastasis of many tumors, including cancers of the brain (e.g. gliomas, glioblastomas, astrocytomas), skin (e.g. melanomas), and neuroendocrine tissues (cancers of the breast, stomach, pancreas, larynx and colon). Because overexpression of NK1R has been reported in most of these malignancies, we have undertaken to design an NK1R-targeted near infrared (NIR) fluorescent dye for fluorescence guided surgeries of these cancers. We demonstrate here that an NK1R-binding ligand linked to the NIR dye LS288 selectively accumulates in NK1R-expressing tumor xenografts with high affinity (K_d = 13 nM), allowing intra-operative imaging of these cancers in live mice. Because tumor accumulation is nearly quantitatively blocked by excess unlabeled ligand, and since NK1R negative tumors and normal tissues display virtually no uptake, we conclude that the observed tumor retention is NK1R mediated. Results on the synthesis, *in vitro* characterization, and animal testing of NK1R-targeted NIR dye are presented.

Introduction

While significant progress has been made on the development of effective chemotherapies for cancer, complete surgical resection is the only reliable cure for cancer to date. Unfortunately, existing surgical approaches fail to enable localization and resection of all malignant lesions, resulting in frequent disease recurrence at the primary tumor site[(1)]. Indeed, up to 40% of breast cancers,(2) 50% of ovarian cancers,(3) 40% of non-small cell lung cancers (NSCLC),(4, 5) 34% of small cell lung cancers,(6) 33% of oral squamous cell carcinomas (OSCC)(7) and 22% of intracranial meningiomas(1) are reported to recur at the site of removal of the original mass. Therefore, there is a need to develop an imaging modality that enables the surgeon to visualize and identify all malignant lesions.

Many imaging modalities such as ultrasound, computed tomography (CT), planar radiography, magnetic resonance imaging (MRI), positron-emission tomography (PET) and single photon emission computed tomography (SPECT) are used to detect diseased tissue in

*Author to whom all correspondence should be addressed: Philip S. Low, plow@purdue.edu, Phone: 765-494-5272.

Supporting Information: The Supporting Information is available free of charge on the ACS Publications website.

Notes: The authors declare no competing financial interest

preparation for surgical intervention.(8-12) However, none of these imaging methods are optimal for informing the surgeon(11, 13) which tissues to resect during surgery due to the fact that: i) the resolution of the imaging methodology may be insufficient to reveal microscopic disease, including positive cancer margins, metastatic lymph nodes, etc., ii) small malignant lesions detected in whole body images can be difficult to locate during the subsequent surgery, iii) the speed of image reconstruction using the selected modality may be too slow for intra-operative decision-making, iv) the required imaging hardware could be too bulky for disease localization in small body cavities, and/or v) the surgeon could be harmed by the accompanying exposure to ionizing radiation.

Based on the many desirable properties of near infrared (NIR) dyes and their associated imaging instrumentation,(14) NIR fluorophores have become the contrast agents of choice for intra-operative imaging.(14-17) Thus, the high spatial resolution of the optical probes, the strong tissue penetrating properties of near-infrared fluorescence (NIRF), the facile ability to target/activate fluorescent dyes specifically in malignant tissues, the small and mobile nature of most optical imaging instruments (e.g. endoscopes),(14) and the real time ability to visualize the diseased tissue all render fluorescence guided surgery the optimal method for intra-operative tumor imaging.(18, 19)

Although existing optical imaging technologies resolve many of the problems associated with non-optical imaging modalities, several aspects of the existing technologies can still be improved.(17) For example, indocyanine green (ICG) has been frequently employed to image solid tumors, presumably because it associates into aggregates or complexes with plasma proteins and accumulates in tumors due to an enhanced permeability and retention (EPR) effect.(19, 20) However, the lack of a significant EPR effect in most slower growing human tumors renders this technique unreliable for human use. Quenched fluorescent pro-dyes that are converted to their fluorescent forms only upon activation by tumor-enriched enzymes (e.g. γ-glutamyl transpeptidase,(21) cathepsin K,(22-24) matrix metalloproteinases 2 and 9,(23-25) etc.) also show promise for optically labeling cancer lesions, however, activation enzyme expression can be heterogeneous in malignant tissues and enzyme upregulation can often be prominent in some nonmalignant tissues. Moreover, the released fluorescent dyes can sometimes diffuse into adjacent healthy tissue, causing the boundary between the malignant and healthy tissue to blur. Finally, usage of fluorescent prodrugs that are only activated under the hypoxic conditions can be exploited to image some hypoxic tumors, but unfortunately many malignant lesions do not contain hypoxic regions.(26, 27)

In order to address the aforementioned limitations in current optical imaging technologies, we have been developing ligand-targeted NIR dyes for cancer surgery.(16, 18, 28) Our choice of using tumor-specific ligands to deliver attached dyes to malignant lesions was motivated by the fact that i) low molecular weight ligands can be designed and synthesized for most receptors that are overexpressed on cancer cells,(28, 29) ii) low molecular weight ligand-targeted dyes can penetrate solid tumors and saturate tumor-specific receptors within minutes of intravenous injection in both animals and humans,(29) iii) ligand-targeted dyes generally clear from receptor negative tissues within one or two hours of post injection,(18, 19) allowing injection of the dye to be performed on the same day as the fluorescence guided surgery, and iv) most ligand targeted dyes are internalized by receptor-mediated

endocytosis, preventing the dye from diffusing into adjacent healthy tissues and retaining the imaging agent within the tumor mass for several days. Finally, because these small molecule targeting ligands are generally nontoxic, it is also possible to repeatedly administer the dye conjugate to the same patient when multiple surgeries are necessary.(18, 30)

In our search for tumor-specific markers, the neurokinin-1 receptor (NK1R) emerged as a promising candidate.(31-34) The physiological ligand of NK1R is termed substance P (SP), which has been shown to induce tumor cell proliferation, angiogenesis, and migration.(35, 36) As a consequence, NK1R is implicated in the growth and metastasis of many tumors, including cancers of the brain (gliomas, glioblastomas, astrocytomas, neuroblastomas)(37, 38), skin, pancreas,(39) eye, larynx, stomach,(40) colon and breast.(35-37, 39, 41) Although NK1R is also present in the healthy brain, receptors in the brain cannot be labeled by these parenterally administered dyes, because the large, hydrophilic, ligand-targeted NIR dye conjugates cannot penetrate the blood brain barrier.(31, 42) Moreover, although NK1R is also expressed by certain epithelial cells, its location on the apical side of these polarized cells renders it accessible to parenterally administered drugs.(31, 43) Thus, the vast majority of accessible NK1R will be found in neuroendocrine cancers that over-express the receptor. In this study, we report the design, development and characterization of a novel NK1 receptor-targeted fluorescent probe for fluorescence guided surgery of neuroendocrine cancers.

Results and Discussions

Synthesis and Evaluation of Binding for NK1RL-Rhodamine (5)

We have repurposed the anticancer drug L-733,060, an NK1R ligand that binds to NK1R with 1 nM affinity, to design an NK1R-targeted fluorescent dye for fluorescence guided surgery of neuroendocrine tumors.(44-46) For initial characterization studies, a short hydrophilic linker (to improve hydrophilicity) was introduced between L-733,060 and rhodamine to create an NK1R-targeted dye **5** that could be easily detected by confocal microscopy and flow cytometry (Scheme 1-3).

Because the ligand is hydrophobic, the hydrophilic linker was chosen to make the overall conjugate hydrophilic and devoid of any non-specific binding and off-targeting. Binding of conjugate **5** to NK1R-transfected HEK293 cells (used as a model for neuroendocrine cancer) was first established by confocal microscopy (Figure 1) and by flow cytometry (Figure 2).

A complete binding curve was then obtained by adding increasing concentrations of **5** to HEK293-NK1R cells in the presence and absence of excess base ligand **3** (Figure 3a). The binding isotherm yielded an apparent K_d= 26 nM and suppression of the majority of binding upon addition of excess unlabeled ligand showed that most of the binding was NK1R-specific. (44, 45) However, it is worth noting that confocal data showed most of the bound **5** remained on the cell surface, even after long exposure times (up to 2h), suggesting that most of the conjugate is not internalized by receptor-mediated endocytosis.

Synthesis and Evaluation of Binding Affinity for NK1RL-Peptide-LS288 (8)—

Having established strong binding and specificity of the NK1R targeted ligand using

rhodamine conjugate, we next designed and tested the NIR dye conjugate **8**, which is expected to enhance the optical visualization in *in vivo* studies due to lack of interference from auto-fluorescence,(19) (Scheme 4 and 5).

Binding affinity of **8** was measured as K_d = 13 nM (Figure 3b) in HEK293-NK1R cells. Competition experiments by pre-incubation with 100-fold excess of base ligand **3** also confirmed receptor mediated uptake of this conjugate (Figure 3b). A combination of strong affinity (K_d =13 nM) and specificity as evidenced by competition experiments prompted us to expect strong binding of the conjugate to the receptors on the tumor, while reducing the off-site toxicity to the healthy organs at low concentration.

In vivo* Evaluation of NK1RL-Peptide-LS288 (8) in NK1R Positive and Negative Tumor Murine Models—In vivo* imaging (Figure 4) and biodistribution (Figure 5) was performed in nu/nu mice with conjugate containing NIR dye **8** in a NK1R-transfected HEK293 tumor xenograft model.

NK1R targeted imaging agents accumulated in tumors 2h post injection by intravenous (*i.v*) administration of dye. Furthermore, no dye accumulation was observed when 100 fold excess of unlabeled base ligand **3** was injected to block all available receptors, confirming the receptor mediated uptake. There was no significant uptake in normal tissues except for kidneys, confirming that NK1R is either not present in sufficient quantity or not accessible on the normal tissue to parenterally administered probes (Figure 4-6).

A low level accumulation in kidneys was observed, which might be due to slow clearing of the dye conjugate. Moreover, the fluorescence intensity in kidneys was not blocked by an excess of non-conjugated ligand suggesting that the uptake was not receptor-mediated. The specificity of targeting was further confirmed by *in vivo* studies using a NK1R-negative tumor (KB cells) xenograft model (right panel of Figure 4 & 5), where the images showed no dye accumulation.

Earlier studies on imaging modalities of NK1 receptor expressing xenografts showed use of peptide and non-peptidic antagonists for several radiologic studies.(47, 48) To the best of our knowledge, this is the first report on the use of non-peptidic (small molecule) antagonists for intra-operative surgery of NK1R expressing cancers in mice xenografts model. This is noteworthy given that non-peptidic small molecule ligands are preferred where in vivo stability of peptides towards proteolytic cleavage is a concern (49, 50).

Conclusions

Targeted fluorescence imaging is a promising technique for early cancer detection and therapy, but remains a challenge in the development of suitable NIR fluorescence probes. In this study, we have demonstrated the design, synthesis, and application of a new targeting ligand that is selective for NK1R-expressing tumors in mouse models. Under the established protocols, we were able to resect tumors using NIR imaging with the LS288-Ligand probe **8**. It provides a simple, rapid, low-cost, highly stable, non-radioactive dye, and highly translatable approach for improved intra-operative NK1 receptor positive tumor visualization and resection. It has the potential to serve as an imaging platform for non-invasive cancer

detection and drug efficacy evaluation studies. Further studies such as radioimaging modalities, SPECT, PET imaging and therapeutic results warrant further investigation.

Materials and Methods

Chemicals

All amino acids were purchased from ChemImpex Intl. (Chicago, IL). HC Matrigel was obtained from BD Biosciences (San Jose, CA). H-Lys (Boc)-2-Cl-Trt resin was purchased from Novabiochem (San Diego, CA). NHS-Rhodamine ester was purchased from Thermo Fisher Scientific Inc., Chicago, Illinois. (Benzotriazol-1-yloxy)tripyrrolidinophosphonium hexafluoro-phosphate (PyBOP) was obtained from Genscript Inc. (Piscataway, New Jersey). The ligand, (*2S*,*3S*)-3-((3,5-bis(trifluoromethyl)benzyl)-oxy)-2-phenylpiperidine (L-733, 060, **1**) was synthesized according to the published procedure. (49) [30,51] (Mizuta and Onomura 2012) [49] Tetrahydrofuran (THF), dichloromethane (CH_2Cl_2) were distilled from calcium hydride. Diisopropylethylamine (DIPEA), piperidine, dimethylformamide (DMF), isopropyl alcohol (i-PrOH), and all other chemicals and reagents were purchased from Sigma Aldrich. LS288 was a gift from Dr. Samuel Achilefu (Washington University, St. Louis, MO).

Cell Culture and Animal Husbandry

HEK293 cell lines stably transfected with neurokinin-1 receptor (NK1R) were utilized in our studies and were donated by Dr. Steven D Douglas, Children's Hospital of Philadelphia, Philadelphia, PA. Cell lines were cultured in Dulbecco's modified Eagle's medium (GIBCO) supplemented with 10% fetal bovine serum, 400 μg/mL of G418 disulfate (Sigma Aldrich), and 1% penicillin streptomycin at 37°C in humidified air enriched with 5% CO_2.

Athymic male nu/nu mice were purchased from Harlan Laboratories (Indianapolis, IN), and maintained on normal rodent chow. They were housed in a sterile environment on a standard 12 h light and dark cycle for the duration of the study. All animal procedures were approved by the Purdue Animal Care and Use Committee (PACUC) in accordance with NIH guidelines.

In vitro Studies

Confocal Laser Scanning Microscopy Image Analysis—HEK293-NK1R cells (50,000 cells/well in 0.5 mL) were seeded into confocal microwell plate (Lab-Tek®, Chambered #1.0 Borosilicate Coverglass) and allowed cells to form monolayers over 48 h. Spent medium was replaced with fresh medium containing NK1R-Lys-Rhodamine (25 nM) in the presence or absence of 100-fold excess base ligand and cells were incubated for 1 h at 37 °C. After washing with fresh medium (3× 0.5 mL), confocal images were acquired using a confocal microscope (FV 1000, Olympus).

Flow Cytometry: Flow Binding Data for NK1R-Lys-Rhodamine—HEK293-NK1R cells were seeded into a T75 flask and allowed to form a monolayer over 48 h. After trypsin digestion, released cells were transferred into centrifuge tubes (1×10^5cells/tube) and centrifuged. The medium was replaced with fresh medium containing NK1RL-Lys-

Rhodamine **5** (25 nM) in the presence or absence of 100-fold excess unlabeled base ligand **3** and incubated for 1h at 37°C. After rinsing with fresh medium (3× 0.5 mL), cells were re-suspended in PBS (0.5 mL) and cell bound fluorescence was analyzed (40,000 cells/sample) using a flow cytometer. Untreated HEK293-NK1R cells in PBS served as a negative control.

Flourimeter: Determination of Binding Affinity and Specificity—HEK293-NK1R cells (50,000 cells/well) were seeded into 24 well plates (BD Purecoat Amine, BD Biosciences) and allowed to grow to confluence over 48–72 h. Spent medium in each well was replaced with 0.5 mL of fresh medium containing 0.5% bovine serum albumin and increasing concentrations of dye conjugates in the presence or absence of 100-fold excess of competing base ligand **3**. After incubation for 1h at 37°C, cells were washed with fresh medium (3 × 0.5 mL) to remove unbound fluorescence and dissolved in 0.5 mL of 1% aqueous sodium dodecyl sulfate (SDS). Cell associated fluorescence was then determined by measuring maximum emission of the resulting solution by transfering to a quartz cuvette upon excitation of dye (rhodamine conjugate at λ_{Ex} 545 nm and LS288 conjugate at 755 nm) using an Agilent Technologies Cary Eclipse fluorescence spectrophotometer. Experiments were performed in triplicate. The conjugate's dissociation constant (K_d) was calculated from a plot of cell bound fluorescence emission (a.u.) versus the concentration of targeted fluorescent probes added using the GraphPad Prism 4 program and assuming a non-cooperative single site binding equilibrium.

In vivo Studies

Implantation of Subcutaneous Tumors in Mice—Six week old male athymic nu/nu mice (Harlan Laboratories, IN) were inoculated subcutaneously on their shoulders with HEK293-NK1R cells (5.0×10^6 cells/mouse in 50% HC Matrigel) or with KB cells (100,000 cells/mouse) using a 25-gauge needle. Growth of the tumors was measured in two perpendicular directions every 2 days using a caliper, and the volumes of the tumors were calculated as $0.5 \times L \times W^2$ (L = measurement of longest axis, and W = measurement of axis perpendicular to L in millimeters). Animals were imaged when the tumors reached 300–500 mm^3 volume (~2-3 weeks). Experiments on live mice involved at least four mice per group. Imaging was then performed as described below.

***In vivo* Fluorescence Imaging—**Tumor bearing mice were treated *via* tail vein (*i.v*) injection with 10 nmoles of dye conjugate (**8**) and imaged 2 h post injection using a Caliper IVIS Lumina II Imaging station coupled to ISOON5160 Andor Nikon camera equipped with Living Image Software Version 4.0. For competition experiments, 100-fold excess of base ligand **3** was used as competition. The 2 h time point for imaging was chosen based on data from previous experiments showing that a radiolabeled NK1RL conjugate yielded the highest tumor-to-background ratio at this time point. The settings were as follows: lamp level, high; excitation, 745 nm; emission, ICG; epi illumination; binning (M) 4; FOV, 12.5; f-stop, 4; acquisition time, 1s. After completion of whole body imaging, animals were dissected and selected organs were collected and imaged again for complete bio-distribution (Figure 5).

Supplementary Material

Refer to Web version on PubMed Central for supplementary material.

Acknowledgments

The support of the following two laboratories is gratefully acknowledged. The gift of HEK293 cells transduced with NK-1R came from Prof. Steven D Douglas, Children's Hospital of Philadelphia, Philadelphia, PA. Dr. Samuel Achilefu (Washington University, St. Louis, MO) provided LS-288. The authors would like to thank John L Harwood and Karl V Wood for nmr and mass spectrometry facilities, respectively and also the Purdue University Center for Cancer Research (PUCCR) for flow cytometry and imaging resources supported by P30 CA023168. This work was supported by funds from Endocyte Inc.

References

1. Konstantinos V, Vasileios K, Pavlos S. The Recurrence Rate in Meningiomas: Analysis of Tumor Location, Histological Grading, and Extent of Resection. Open Journal of Modern Neurosurgery. 2012; 2(1):4.
2. Freedman GM, Fowble BL. Local recurrence after mastectomy or breast-conserving surgery and radiation. Oncology (Williston Park). 2000; 14:1561–81. discussion 1581-2, 1582-4. [PubMed: 11125941]
3. Burger IA, Goldman DA, Vargas HA, Kattan MW, Yu C, Kou L, Andikyan V, Chi DS, Hricak H, Sala E. Incorporation of postoperative CT data into clinical models to predict 5-year overall and recurrence free survival after primary cytoreductive surgery for advanced ovarian cancer. Gynecol Oncol. 2015; 138:554–9. [PubMed: 26093061]
4. Kelsey CR, Higgins KA, Peterson BL, Chino JP, Marks LB, D'Amico TA, Varlotto JM. Local recurrence after surgery for non-small cell lung cancer: a recursive partitioning analysis of multi-institutional data. J Thorac Cardiovasc Surg. 2013; 146:768–773. [PubMed: 23856204]
5. Choi PJ, Jeong SS, Yoon SS. Prognosis of recurrence after complete resection in early-stage non-small cell lung cancer. Korean J Thorac Cardiovasc Surg 2013. 2013; 46:449–56.
6. Lou F, Huang J, Sima CS, Dycoco J, Rusch V, Bach PB. Patterns of recurrence and second primary lung cancer in early-stage lung cancer survivors followed with routine computed tomography surveillance. J Thorac Cardiovasc Surg. 2013; 145:75–81. [PubMed: 23127371]
7. Wang B, Zhang S, Yue K, Wang XD. The recurrence and survival of oral squamous cell carcinoma: a report of 275 cases. Chinese Journal of Cancer. 2013; 32:614–618. [PubMed: 23601241]
8. Fabian K, Jessica B, Stanley F, Monica S, Georg S, Moritz P. Targeted Ultrasound Imaging of Cancer: An Emerging Technology on its Way to Clinics. Curr Pharm Des. 2012; 18:2184–2199. [PubMed: 22352772]
9. Ambrosini V, Fani M, Fanti S, Forrer F, Maecke HR. Radiopeptide imaging and therapy in Europe. J Nucl Med 2011. 2011; 52(Supplement 2):42S–55S.
10. Banerjee SR, Pullambhatla M, Foss CA, Nimmagadda S, Ferdani R, Anderson CJ, Mease RC, Pomper MG. 64Cu-Labeled Inhibitors of Prostate-Specific Membrane Antigen for PET Imaging of Prostate Cancer. J Med Chem. 2014; 57:2657–2669. [PubMed: 24533799]
11. Ibrahim N, Cho SY. Prostate cancer imaging: positron-emission tomography perspectives. Reports in Medical Imaging. 2015; 8:51–62.
12. Frangioni JV. New Technologies for Human Cancer Imaging. J Clin Oncol. 2008; 26:4012–4021. [PubMed: 18711192]
13. Patterson SK. New technologies in breast imaging. J Natl Compr Cancer Network. 2003; 1(2):272–278.
14. Frangioni JV. In vivo near-infrared fluorescence imaging. Curr Opin Chem Biol. 2003; 7:626–34. [PubMed: 14580568]
15. Huang R, Vider J, Kovar JL, Olive DM, Mellinghoff IK, Mayer-Kuckuk P, Kircher MF, Blasberg RG. Integrin alphavbeta3-targeted IRDye 800CW near-infrared imaging of glioblastoma. Clin Cancer Res 2012. 2012 Oct 15; 18(20):5731–40.

16. Kelderhouse LE, Chelvam V, Wayua C, Mahalingam S, Poh S, Kularatne SA, Low PS. Development of tumor-targeted near infrared probes for fluorescence guided surgery. Bioconjugate Chem. 2013; 24:1075–1080.
17. Snoeks TJ, van Driel PB, Keereweer S, Aime S, Brindle KM, van Dam GM, Lowik CW, Ntziachristos V, Vahrmeijer AL. Towards a successful clinical implementation of fluorescence-guided surgery. Mol Imaging Biol. 2013; 16(2):147–151.
18. van Dam GM, Themelis G, Crane LM, Harlaar NJ, Pleijhuis RG, Kelder W, Sarantopoulos A, de Jong JS, Arts HJ, van der Zee, et al. Intraoperative tumor-specific fluorescence imaging in ovarian cancer by folate receptor-alpha targeting: first in-human results. Nat Med 2011. 2011 Sep 18; 17(10):1315–9.
19. Nguyen QT, Tsien RY. Fluorescence-guided surgery with live molecular navigation--a new cutting edge. Nat Rev Cancer. 2013; 13:653–62. [PubMed: 23924645]
20. Jain RK, Stylianopoulos T. Delivering nanomedicine to solid tumors. Nat Rev Clin Oncol. 2010; 7:653–664. [PubMed: 20838415]
21. Urano Y, Sakabe M, Kosaka N, Ogawa M, Mitsunaga M, Asanuma D, Kamiya M, Young MR, Nagano T, Choyke PL, et al. Rapid Cancer Detection by Topically Spraying a gama-Glutamyltranspeptidase- Activated Fluorescent Probe. Sci Transl Med. 2011; 3:110ra119–110ra119.
22. Kozloff KM, Quinti L, Patntirapong S, Hauschka PV, Tung CH, Weissleder R, Mahmood U. Non-Invasive Optical Detection of Cathepsin K-Mediated Fluorescence Reveals Osteoclast Activity In Vitro and In Vivo. Bone. 2009; 44:190–198. [PubMed: 19007918]
23. Bremer C, Tung CH, Weissleder R. In vivo molecular target assessment of matrix metalloproteinase inhibition. Nat Med. 2001; 7:743–8. [PubMed: 11385514]
24. Yhee JY, Kim SA, Koo H, Son S, Ryu JH, Youn IC, Choi K, Kwon IC, Kim K. Optical imaging of cancer-related proteases using near-infrared fluorescence matrix metalloproteinase-sensitive and cathepsin B-sensitive probes. Theranostics. 2012; 2:179–89. Epub 2012 Feb 10. DOI: 10.7150/thno.3716 [PubMed: 22375156]
25. Fudala R, Ranjan AP, Mukerjee A, Vishwanatha JK, Gryczynski Z, Borejdo J, Sarkar P, Gryczynski I. Fluorescence Detection of MMP-9. I. MMP-9 Selectively Cleaves Lys-Gly-Pro-Arg-Ser-Leu-Ser-Gly-Lys Peptide. Curr Pharm Biotechnol. 2011; 12:834–838. [PubMed: 21446907]
26. Metran-Nascente C, Yeung I, Vines D, Metser U, Dhani N, Green D, Milosevic M, Jaffray D, Hedley D. Measurement of tumor hypoxia in patients with advanced pancreatic cancer based on 18F-fluoroazomyin arabinoside (18F-FAZA) uptake. J Nucl Med. 2016; 57(3):361–366. [PubMed: 26769863]
27. Erkan M, Kurtoglu M, Kleeff J. The role of hypoxia in pancreatic cancer: a potential therapeutic target? Expert Rev Gastroenterol Hepatol. 2015; 27:1–16.
28. Wayua C, Low PS. Evaluation of a cholecystokinin 2 receptor-targeted near-infrared dye for fluorescence-guided surgery of cancer. Mol pharmaceutics. 2013; 11(2):468–476.
29. Low PS, Henne WA, Doorneweerd DD. Discovery and Development of Folic-Acid-Based Receptor Targeting for Imaging and Therapy of Cancer and Inflammatory Diseases. Acc Chem Res. 2008; 41:120–129. [PubMed: 17655275]
30. Srinivasarao M, Galliford CV, Low PS. Principles in the design of ligand-targeted cancer therapeutics and imaging agents. Nat Rev Drug Discovery. 2015; 14:203–219. [PubMed: 25698644]
31. Grachev P, Millar RP, O'Byrne KT. The Role of Neurokinin B Signalling in Reproductive Neuroendocrinology. Neuroendocrinology 2013. 2013 Dec 17.
32. Ballet S, Feytens D, Buysse K, Chung NN, Lemieux C, Tumati S, Keresztes A, Van Duppen J, Lai J, Varga E, et al. Design of novel neurokinin 1 receptor antagonists based on conformationally constrained aromatic amino acids and discovery of a potent chimeric opioid agonist-neurokinin 1 receptor antagonist. J Med Chem. 2011; 54:2467–2476. [PubMed: 21413804]
33. Di Fabio R, Alvaro G, Griffante C, Pizzi DA, Donati D, Mattioli M, Cimarosti Z, Guercio G, Marchioro C, Provera S, et al. Discovery and Biological Characterization of (2R,4S)-1′-Acetyl-N-{(1R)-1-[3,5-bis(trifluoromethyl)phenyl]ethyl}-2-(4-fluoro-2-methylphenyl)-N-methyl-4,4′-

bipiperidine-1-carboxamide as a New Potent and Selective Neurokinin 1 (NK1) Receptor Antagonist Clinical Candidate. J Med Chem. 2011; 54:1071–1079. [PubMed: 21229983]

34. Rosso M, Muoz M, Berger M. The Role of Neurokinin-1 Receptor in the Microenvironment of Inflammation and Cancer. The Scientific World Journal. 2012; 2012:21.
35. Munoz M, Covenas R. Neurokinin-1 receptor: a new promising target in the treatment of cancer. Discov Med 2010. 2010; 10:305–13.
36. Munoz M, Covenas R. Involvement of substance P and the NK-1 receptor in cancer progression. Peptides. 2013; 48:1–9. [PubMed: 23933301]
37. Munoz M, Rosso M. The NK-1 receptor antagonist aprepitant as a broad spectrum antitumor drug. Invest New Drugs. 2010; 28:187–93. [PubMed: 19148578]
38. Fowler CJ, Brannstrom G. Substance P enhances forskolin-stimulated cyclic AMP production in human UC11MG astrocytoma cells. Methods Find Exp Clin Pharmacol. 1994; 16:21–28. [PubMed: 7513037]
39. Friess H, Zhu Z, Liard V, Shi X, Shrikhande SV, Wang L, Lieb K, Korc M, Palma C, Zimmermann A, et al. Neurokinin-1 receptor expression and its potential effects on tumor growth in human pancreatic cancer. Lab Invest. 2003; 83(5):731–42. [PubMed: 12746482]
40. Feng F, Yang J, Tong L, Yuan S, Tian Y, Hong L, Wang W, Zhang H. Substance P immunoreactive nerve fibres are related to gastric cancer differentiation status and could promote proliferation and migration of gastric cancer cells. Cell Biol Int. 2011; 35:623–9. [PubMed: 21091434]
41. Schulz S, Stumm R, Rocken C, Mawrin C, Schulz S. Immunolocalization of Full-length NK1 Tachykinin Receptors in Human Tumors. J Histochem Cytochem. 2006; 54:1015–1020. [PubMed: 16651388]
42. Jiang J, Bunda JL, Doss GA, Chicchi GG, Kurtz MM, Tsao KLC, Tong X, Zheng S, Upthagrove A, Samuel K, et al. Potent, Brain-Penetrant, Hydroisoindoline-Based Human Neurokinin-1 Receptor Antagonists. J Med Chem. 2009; 52:3039–3046. [PubMed: 19354254]
43. Abey HT, Fairlie DP, Moffatt JD, Balzary RW, Cocks TM. Protease-Activated Receptor-2 Peptides Activate Neurokinin-1 Receptors in the Mouse Isolated Trachea. J Pharmacol Exp Ther. 2006; 317:598–605. [PubMed: 16434565]
44. Di Fabio R, Alvaro G, Braggio S, Carletti R, Gerrard PA, Griffante C, Marchioro C, Pozzan A, Melotto S, Poffe A, et al. Identification, biological characterization and pharmacophoric analysis of a new potent and selective NK1 receptor antagonist clinical candidate. Bioorg Med Chem. 2013; 21:6264–6273. [PubMed: 24075145]
45. Ladduwahetty T, Baker R, Cascieri MA, Chambers MS, Haworth K, Keown LE, MacIntyre DE, Metzger JM, Owen S, Rycroft W, et al. N-Heteroaryl-2-phenyl-3-(benzyloxy)piperidines: A Novel Class of Potent Orally Active Human NK1 Antagonists. J Med Chem. 1996; 39:2907–2914. [PubMed: 8709125]
46. Pansare SV, Paul EK. Synthesis of (+)-L-733,060, (+)-CP-99,994 and (2S,3R)-3-hydroxypipecolic acid: application of an organocatalytic direct vinylogous aldol reaction. Org Biomol Chem. 2012; 10:2119–25. [PubMed: 22294285]
47. Cordier D, Gerber A, Kluba C, Bauman A, Hutter G, Mindt TL, Mariani L. Expression of Different Neurokinin-1 Receptor (NK1R) Isoforms in Glioblastoma Multiforme: Potential Implications for Targeted Therapy. Cancer Biother Radiopharm. 2014; 29:221–226. [PubMed: 24552486]
48. Hietala J, Nyman MJ, Eskola O, Laakso A, Gronroos T, Oikonen V, Bergman J, Haaparanta M, Forsback S, Marjamaki P, et al. Visualization and quantification of neurokinin-1 (NK1) receptors in the human brain. Mol Imaging Biol. 2005; 7:262–72. [PubMed: 16155744]
49. Otvos L, Wade JD. Current challenges in peptide-based drug discovery. Frontiers in chemistry. 2014; 2:62. [PubMed: 25152873]
50. Fosgerau K, Hoffmann T. Peptide therapeutics: current status and future directions. Drug discovery today. 2015; 20(1):122–128. [PubMed: 25450771]
51. Mizuta S, Onomura O. Diastereoselective addition to N-acyliminium ions with aryl- and alkenyl boronic acids via a Petasis-type reaction. RSC Advances. 2012; 2:2266–2269.

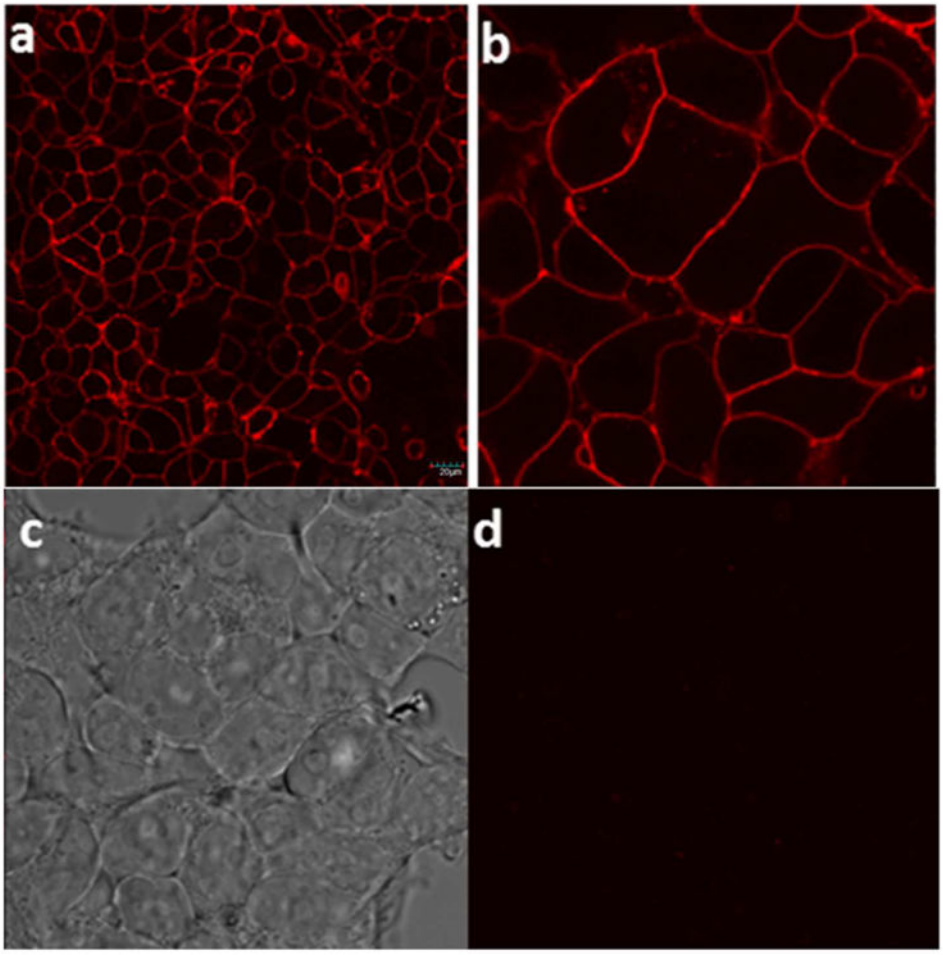

Figure 1.

Confocal microscopy images: In vitro binding studies of NKl-Lys-Rhodamine **5** conjugate to HEK293-NK1R cells, (a) Incubation of cells for 1 h at 37 °C with 25 nM of **5** (b) Image (a) under 3× magnification (c) Image (b) under white light (d) Incubation with 25 nM of **5** in presence of 100-fold excess of competing base ligand). **Scale bar = 20 μm**

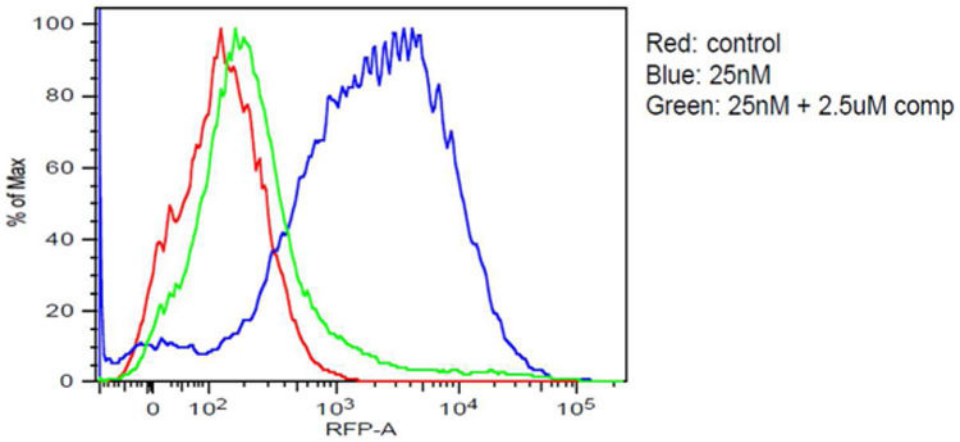

Figure 2.

Binding of NKIRL-Lys-Rhodamine **5** to HEK293-NK1R cells by flow cytometry. Colors from the graph : Red- control (no conjugate added), Blue- (dye conjugate **5** added) and Green- (dye conjugate + 100× competing base ligand **3** added).

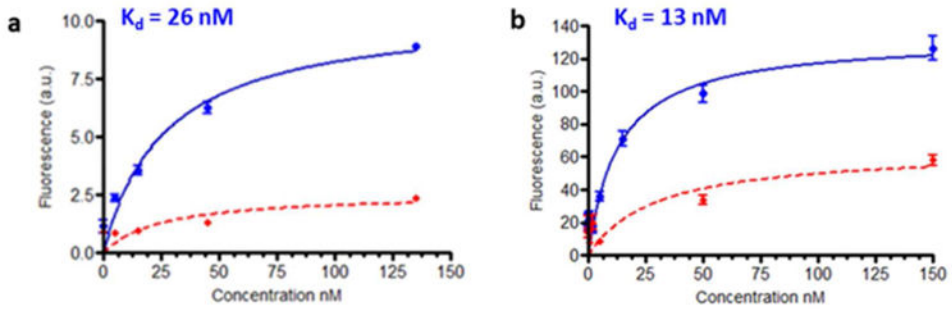

Figure 3.

Fluorescence binding affinity study of (a) NKIRL-Lys-Rhodamine and **5** (b) NKlRL-Peptide-LS288 **8** conjugates in cultured HEK293-NK1R cells in the absence (blue) and in the presence (red) of lOO× of competing base ligand **3**.

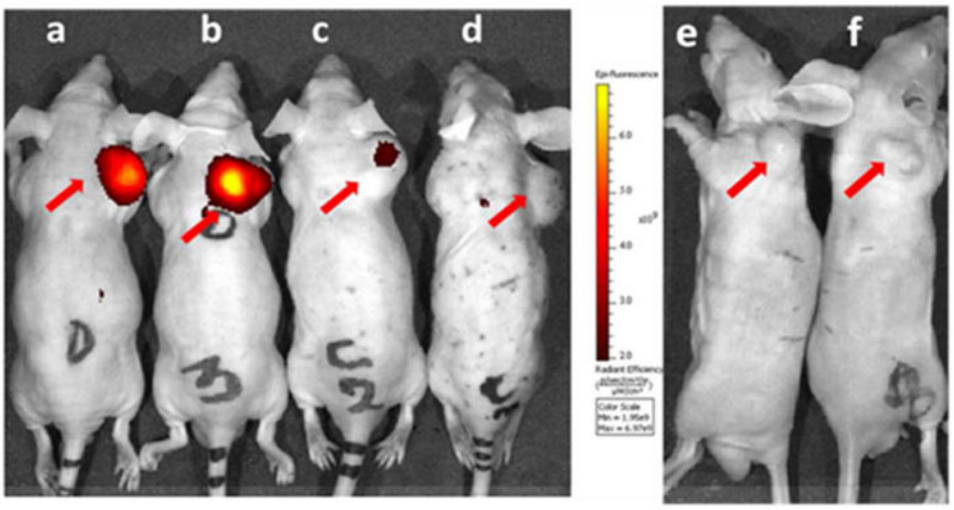

Figure 4.

Whole body imaging of tumor-bearing mice 2h following tail vein injection of 2 nmol of NKlRL-Peptide-LS288. Mice implanted with a NK1R tumor (a-d) and KB tumor (e-f) were injected NKlRL-Peptide-LS288 in the absence (a, b, e, f) or presence (c, d) of 100-fold excess of ligand **3**. Note that KB tumors express no NK1 receptor (negative control). Tumors are shown with red arrows.

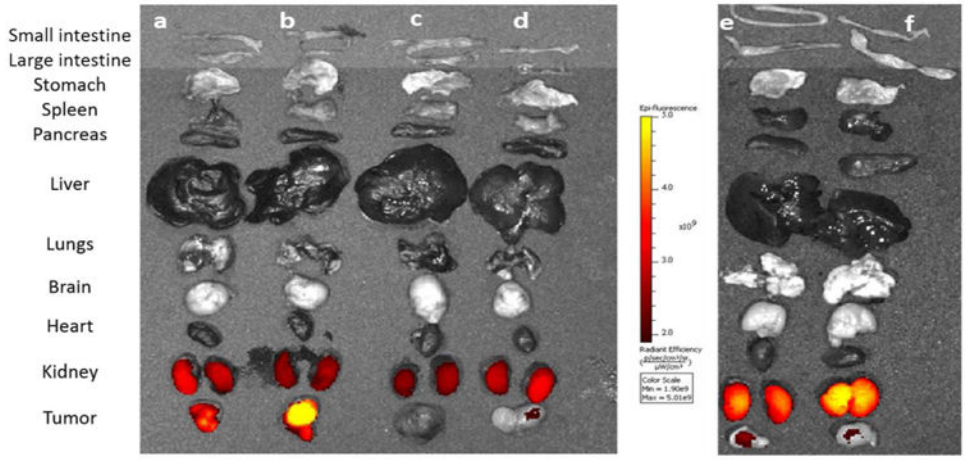

Figure 5.

Evaluation of NKlRL-Peptide-LS288 accumulation in the internal tissues and organs of the mice shown in Figure 4. Mice implanted with a NK1R tumor (a-d) and KB tumor (e-f) was injected NKlRL-Peptide-LS288 in the absence (a, b, e, f) or presence (c, d) of 100-fold excess of base ligand to block all vacant receptor binding sites.

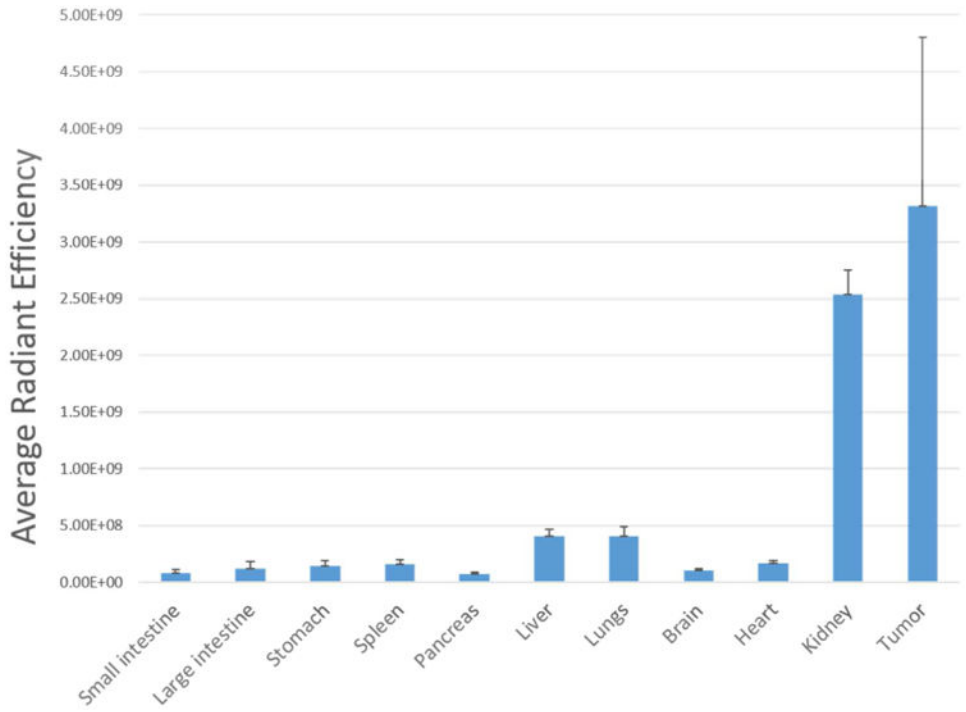

Figure 6.

Quantitative biodistribution of NKlRL-Peptide-LS288 in the NK1R tumor, internal tissues and organs of the treated group of mice shown in Figure 5. (n=4)

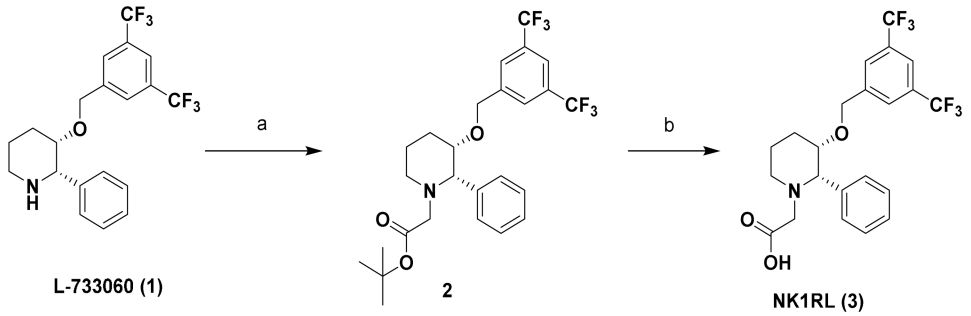

L-733060 (1) 2 NK1RL (3)

Scheme 1.

Synthesis of NK1RL: (a) Ethyl bromoacetate, Triethylamine, THF, rt, 16 h, 92 %; (b) Trifluoroacetic acid, CH_2Cl_2, rt, 4 h, 90 %.

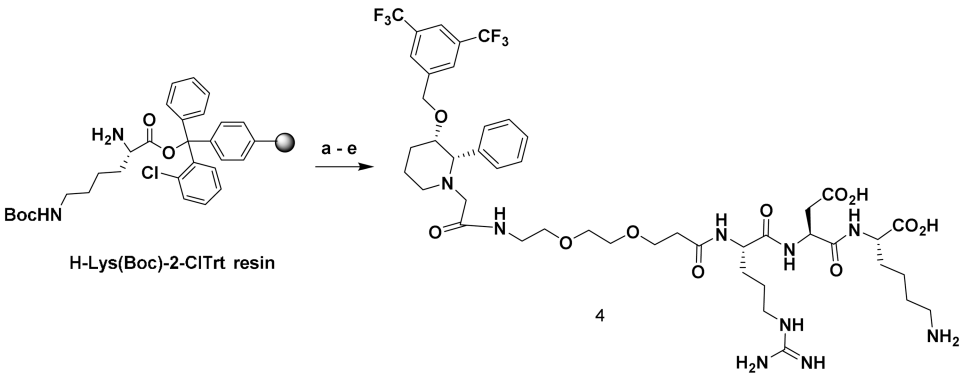

Scheme 2.

Synthesis of NK1RL-Lys Linker, 4. Reagents and conditions: (a) (i) DCM, DMF wash, (ii) Fmoc-Asp(OtBu)-OH, PyBOP, DIPEA, DMF, 4 h; (b) (i) 20% piperidine in DMF, 3×10 min, (ii) Fmoc-Arg(pbf)-OH, PyBOP, DIPEA, DMF, 4 h; (c) (i) 20% piperidine in DMF, 3×10 min, (ii) Fmoc-PEG_2-OH, PyBOP, DIPEA, DMF, 4 h; (d) L-733 060-AcOH, PyBOP, DIPEA, DMF, 12 h (e) TFA:H_2O:TIPS, 95:2.5:25, 3×15 min, 26 %.

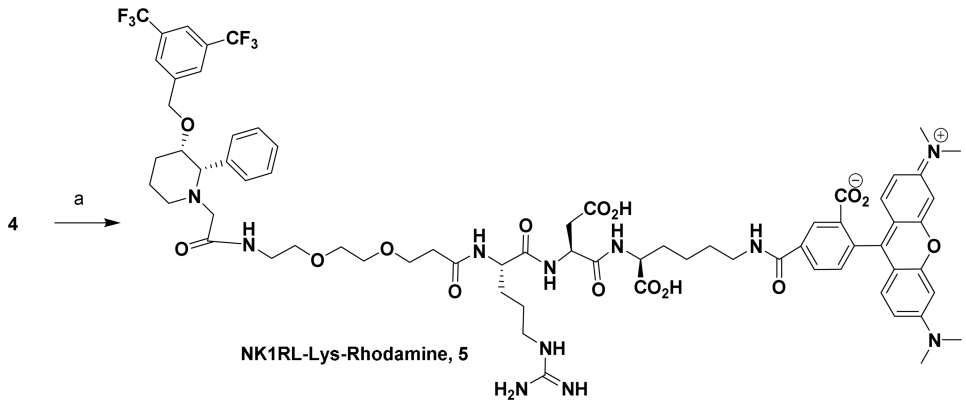

Scheme 3.

Synthesis of NK1RL-Lys-Rhodamine (5): Reagents and Conditions: (a) NHS-Rhodamine, DIPEA, DMSO, rt, 12 h, 65 %.

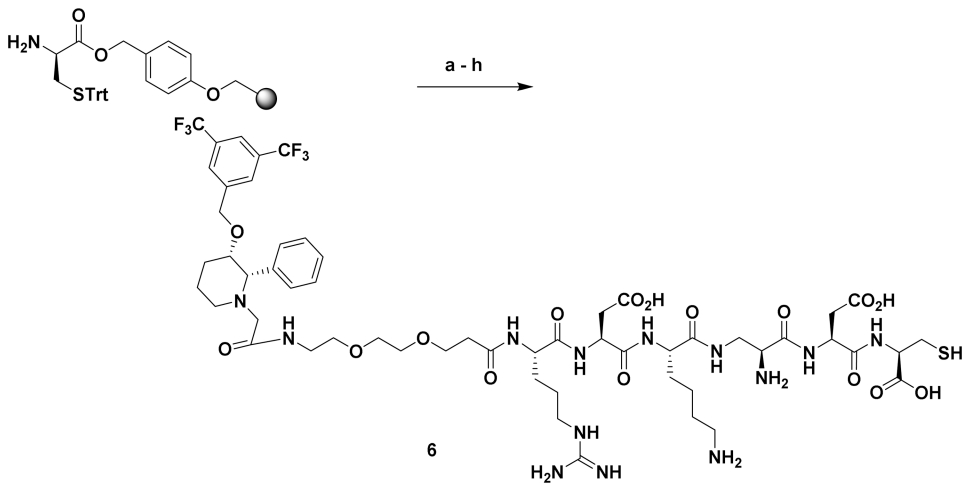

Scheme 4.

Synthesis of NK1RL-Peptide Linker (6): Reagents and conditions:(a) (i) DCM, DMF wash, (ii) Fmoc-Asp(OtBu)-OH, PyBOP, DIPEA, DMF, 4 h; (b) (i) 20% piperidine in DMF, 3×10 min, (ii) Boc-DAP(Fmoc)-OH, PyBOP, DIPEA, DMF, 4 h; (c) (i) 20% piperidine in DMF, 3×10 min, (ii) Fmoc-Lys(Boc)-OH, PyBOP, DIPEA, DMF, 4 h; (d) (i) 20% piperidine in DMF, 3×10 min, (ii) Fmoc-Asp(OtBu)-OH, PyBOP, DIPEA, DMF, 4 h; (e) (i) 20% piperidine in DMF, 3×10 min, (ii) Fmoc-Arg(pbf)-OH, PyBOP, DIPEA, DMF, 4 h; (f) (i) 20% piperidine in DMF, 3×10 min, (ii) Fmoc-PEG_2-OH, PyBOP, DIPEA, DMF, 4 h; (g) (i) 20% piperidine in DMF, 3×10 min, (ii) L-733060-AcOH, PyBOP, DIPEA, DMF, 12 h; (h) TFA:H_2O:TIPS:EDT, 92.5:2.5:2.5:2.5, 3×5 mL × 15 min, 38 %.

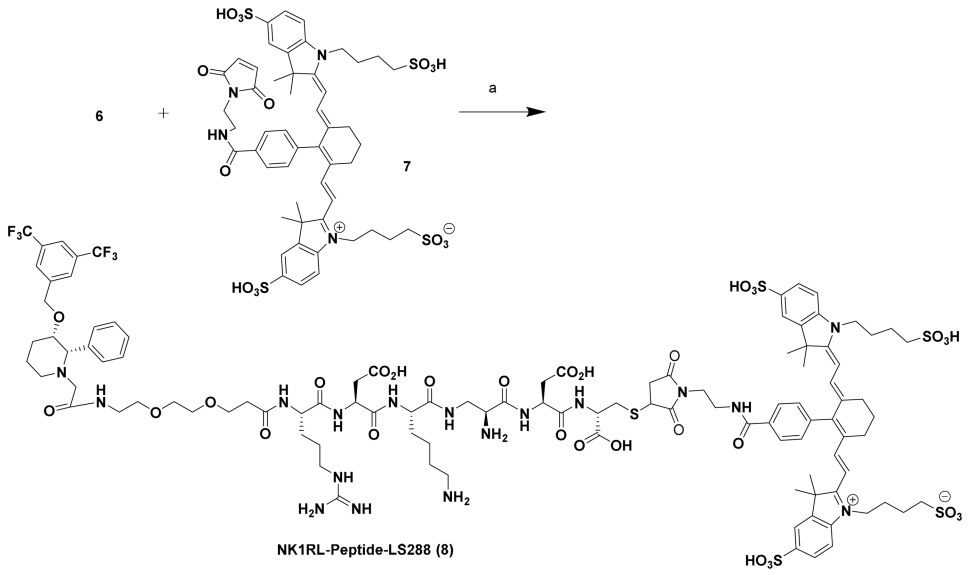

Scheme 5.

Synthesis of NK1RL-Peptide-LS288 Conjugate (**8**): Reagents and conditions: (a) LS-288-Maleimide, (**7**), DIPEA, DMSO, rt, 12 h, 22 %.